Proximity effects of vortices in neutron $^3P_2$ superfluids in neutron stars: Vortex core transitions and covalent bonding of vortex molecules

Michikazu Kobayashi
School of Engineering Science, Kochi University of Technology, Miyanoguchi 185, Tosayamada, Kami, Kochi 782-8502, Japan

Muneto Nitta
Department of Physics, and Research and Education Center for Natural Sciences, Keio University, Hiyoshi 4-1-1, Yokohama, Kanagawa 223-8521, Japan
and International Institute for Sustainability with Knotted Chiral Meta Matter, Hiroshima University, 1-3-2 Kagamiyama, Higashi-Hiroshima, Hiroshima 739-8511, Japan

(Received 20 October 2022; revised 9 February 2023; accepted 17 March 2023; published 4 April 2023)

Neutron $^3P_2$ superfluids consisting of neutron pairs with the total angular momentum $J = 2$, spin-triplet, and P wave are believed to be realized in neutron star cores. Within the Ginzburg-Landau theory it was previously found that a singly quantized vortex is split into two half-quantized non-Abelian vortices connected by one (or three) soliton(s) forming a vortex molecule with the soliton bond(s), in the absence (presence) of a magnetic field parallel to them. In this paper, we investigate proximity effects of two vortex molecules by exhausting all possible two vortex molecule states consisting of four half-quantized vortices and determine the phase diagram spanned by the magnetic field and rotation speed. As the rotation speed is increased, the distance between the two vortex molecules becomes shorter. In the magnetic field below the critical value, we find that as the rotation speed is increased, the two separated vortex molecules transit to a dimerized vortex molecule, where the two vortex molecules are bridged by two solitons that we call "covalent bonds" in analogy with chemical molecules. We also find that the orders of the constituent half-quantized vortex cores transit from a ferromagnetic order to a cyclic order as the vortex molecules come closer. On the other hand, no dimerization occurs in the magnetic field above the critical value. Instead, we find a transition for the polarization direction of the vortex molecules from a configuration parallel to the separation to one perpendicular to the separation as they come closer. We also show some examples of three, four, and many vortex molecule states.

DOI: 10.1103/PhysRevC.107.045801

I. INTRODUCTION

Neutron stars are rapidly rotating extremely high density compact stars accompanied with strong magnetic fields. Recently, there have been great progresses in astrophysical observations of neutron stars (pulsars), such as massive neutron stars with masses about twice as large as the solar mass [1,2], detection of gravitational waves from a binary neutron star merger [3,4], and the Neutron star Interior Composition Explorer (NICER) mission [5,6]. These are providing us astrophysical laboratories for exploring nuclear and quantum chromodynamics (QCD) matter under extreme conditions: extremely high density, with strong magnetic fields and under rapid rotations [7,8].

It is believed that the interior of neutron stars exhibit neutron superfluidity and proton superconductivity [9], see Refs. [7,10–14] as a review. Such supercomponents provide low-energy excitations affecting several processes and properties of neutron stars: neutrino emissivities and specific heats relevant to the long relaxation time after pulsar glitches (sudden speed-up events of neutron stars) [15–17], and the enhancement of neutrino emission around the critical point of the superfluid transition [18–23]. In addition to these, vortices have quantized circulations due to the Feynman-Onsager's quantization in order for the wave function to be single-valued, and thus are called quantum vortices. As a result, rotating superfluids possess a large number of quantum vortices along the rotation axis, forming a vortex lattice. In typical neutron stars, there should exist 10^{17} quantum vortices, considered to play significant roles in neutron star dynamics. For instance, the origin of pulsar glitches was suggested to be explained by avalanche unpinning of a large number of quantum vortices [24,25].

At lower density corresponding to outer cores of neutron stars, Cooper pairs of neutrons responsible for neutron superfluidity are realized due to the attraction by the $^1S_0$ channel between two neutrons [26]. On the other hand, at higher density corresponding to the inner cores of neutron stars, the $^1S_0$ channel becomes repulsive due to the strong short-range repulsion. Instead, the $^3P_2$ channel originating from a strong spin-orbit force at large scattering energy becomes more dominant, where neutron Cooper pairs possess a spin-triplet and P wave with the total angular momentum $J = 2$ [27–44]. Furthermore, the $^3P_2$ channel is tolerant against the strong magnetic field such as 10^{15}–10^{18} G for magnetars, because aligned Cooper pairs with the spin-triplet pairing are not broken by the Zeeman effect, in contrast to the S-wave Cooper

TABLE I. Properties of $^3P_2$ superfluids in the absence and presence of the magnetic field below and above the critical magnetic field B_c. (a) Phases in the bulk, (b) unbroken symmetries in the bulk, (c) OPMs corresponding to the symmetry breakings, (d) the first homotopy groups of the OPMs supporting vortices, (e) the order inside cores of half-quantized vortices, (f) the number of solitons connecting two half-quantized vortices consisting of a singly quantized vortex, and (g) the order of soliton cores are summarized. In row (d), $\mathbb{Q} = D_2^*$ is a quaternion group as the universal covering group of D_2 with the asterisk $*$ denoting the universal covering, and $\rtimes_h$ is a product defined in Ref. [83], supporting the isolated half-quantized non-Abelian vortices in the D_4BN phase. The brackets in rows (e) and (f) and the column $|\boldsymbol{B}| = 0$ represent a metastable solution. The most parts of this table are taken from our previous paper [80].

	$\lvert\boldsymbol{B}\rvert = 0$	$0 < \lvert\boldsymbol{B}\rvert < B_c$	$B_c < \lvert\boldsymbol{B}\rvert$
(a) Phase	UN	D_2BN	D_4BN
(b) Symmetry	O(2)	D_2	D_4
(c) OPM	$S^1 \times \mathbb{R}P^2$	$\mathrm{U}(1) \times \frac{\mathrm{SO}(3)}{D_2}$	$\frac{\mathrm{U}(1)\times\mathrm{SO}(3)}{D_4}$
(d) π_1(OPM)	$\mathbb{Z} \oplus \mathbb{Z}_2$	$\mathbb{Z} \oplus \mathbb{Q}$	$\mathbb{Z} \rtimes_h D_4^*$
(e) Vortex core order	Ferro (Cyclic)	Cyclic	Cyclic
(f) # of solitons	1 (3)	3	3
(g) Soliton core order	D_4BN	D_4BN	D_2BN

pairs which can survive at most around the magnetic field 10^{17} G [45]. In astrophysical observations, the rapid cooling of the neutron star in Cassiopeia A was proposed to be explained by the enhancement of neutrino emissivities due to the formation and dissociation of neutron $^3P_2$ Cooper pairs [21–23].

Theoretically, there are two frameworks to deal with the $^3P_2$ superfluids related to each other: a microscopic theory known as the Bogoliubov–de Gennes (BdG) equation describing fermion degrees of freedom, and the Ginzburg-Landau (GL) theory for the order parameters conveniently describing bosonic excitations. The latter can be obtained from the former by integrating out fermion degrees of freedom as an expansion of the order parameters and spatial derivatives. Thus, the GL theory is the low-energy effective theory describing large distance behaviors, which is valid only in the region close to the critical temperature. Among superfluid states with $J = 2$ classified into nematic, cyclic, and ferromagnetic phases, etc. [46], the GL theory for $^3P_2$ superfluids [32,33,47–55] predicts that the ground state is in the nematic phase at least in the weak coupling limit [47–49].[1] The nematic phase consists of almost degenerate three different states with different unbroken symmetries: uniaxial nematic (UN), D_2 biaxial nematic (D_2BN), and D_4 biaxial nematic (D_4BN) phases with unbroken groups O(2), D_2 and D_4, respectively. Here, D_n is a dihedral group of order n [see Table I(a) and I(b)]. Depending on the magnetic field and temperature, the UN, D_2BN, or D_4BN state is realized as the ground state for zero magnetic field, nonzero one below the critical value B_c, or nonzero one above B_c, respectively [51,53–55] [see Table I(a)]. Apart from nematic phases, more general uniform states (which do not have to be realized as the ground states) of $^3P_2$ superfluids were classified according to symmetries [56]. In fact, beyond the quasiclassical approximation, the ferromagnetic phase was found in the region close to the critical temperature [57]. The GL approach is useful not only to determine the ground states but also to deal with bosonic collective excitations [58–70] relevant for the cooling process of neutron stars, and various topological excitations and defects, such as vortices (as explained below in more detail), domain walls [71], and the boundary defect (boojums) [72].

On the other hand, the BdG approach offers a microscopic description with fermion degrees of freedom valid at short distances and all ranges of temperatures including zero temperature [57,73–76]. It was applied to the phase diagram of $^3P_2$ superfluids in the plane of the temperature and magnetic field, which is valid even at zero temperature [73], including a tricritical point connecting first and second order phase transition lines between D_4 and D_2BN phases [73,74]. Furthermore, $^3P_2$ superfluids were shown to be topological superfluids of a class DIII in the classification of topological insulators and superconductors [77,78], ensuring a topologically protected gapless Majorana fermion on its boundary [73] and inside vortex cores [75,76] as explained below.

Since it is promising that quantum vortices in S-wave superfluids play significant roles in neutron star dynamics, the same should be expected for the $^3P_2$ superfluids as well. In fact, quantum vortices were investigated in the case of $^3P_2$ superfluids both in the GL theory [32,48,49,51,52,79,80] (coreless vortices [81]) and in the BdG theory [75,76]. The first homotopy group classifies types of vortices in each phase [51] as in Table I(d). Singly quantized vortices in $^3P_2$ superfluids were studied in the GL theory [32,48,49,51,79] and in the BdG theory [75] with topologically protected Majorana fermions in the vortex cores. Vortices more peculiar to the $^3P_2$ superfluids are half-quantized non-Abelian vortices [52,76,80], which have a half of the Feynman-Onsager's quantized circulations and are characterized by a non-Abelian first homotopy group D_4^*, thus giving noncommutativity when exchanging two vortices. Isolated half-quantized non-Abelian vortices are topologically allowed only in the D_4BN phase. The existence of half-quantized vortices was proposed to explain a scaling law of pulsar glitches [82]. While an axisymmetric ansatz was employed in the previous studies of vortex solutions [32,48,49,51,52,79], it was shown in the BdG equation [76] that a singly quantized vortex always splits into two half-quantized non-Abelian vortices with any strength of the magnetic field, forming a vortex molecule[2] It was also found in Ref. [76] that a Majorana fermion zero mode is

[1] Among $J = 2$ superfluids, nematic phases are also known in spin-2 Bose-Einstein condensates (BECs) of ultracold atomic gases [56,90,99–102], and thus they have common bosonic properties.

[2] Similar molecules of half-quantized vortices connected by a linear soliton are present in the other multicomponent condensed matter physics and high energy physics: multicomponent or multigap superconductors [109–122], coherently coupled multicomponent BECs [85–87,92,93,123–133], high density QCD [134], and two-Higgs doublet models [135]. However, the unique feature of $^3P_2$ superfluids

TABLE II. The values of the U(1) × SO(3) invariants $\boldsymbol{S}^2$, $|\Psi_{20}|^2$, and $|\Psi_{30}|^2$ for ferromagnetic (F), uniaxial nematic (UN), D_4 biaxial nematic (BN), D_2BN, and cyclic (C) states.

Phase	$\boldsymbol{S}^2/\rho^2$	$\lvert\Psi_{20}\rvert^2/\rho^2$	$\lvert\Psi_{30}\rvert^2/\rho^3$
F	4	0	0
UN	0	1	1
D_4BN	0	1	0
D_2BN	0	1	(0,1)
C	0	0	2

trapped in each half-quantized vortex. Such a splitting of a singly quantized vortex was also confirmed in the GL theory without enforcing axisymmetry [80]. In the GL theory, cores of two half-quantized vortices exhibit a ferromagnetic order in the UN phase with the zero magnetic field, and a cyclic order in the D_2 and D_4BN phases in the presence of the magnetic field, as summarized in Table I(e). In the UN phase in the absence of the magnetic field, the most stable singly quantized vortex configuration consists of two half-quantized vortices with the ferromagnetic cores connected by a single soliton of the D_4BN order. In addition to this, there is also a metastable configuration consisting of those of the cyclic cores connected by three solitons of the D_4BN order. On the other hand, in the D_2 (D_4)BN phase in the presence of small (large) magnetic field, two half-quantized vortices are connected by three linear solitons of the D_4 (D_2)BN order. [See Table I(f) and I(g).] Even in the bulk UN and D_2BN phases, the D_4BN order locally appears around the vortex cores as solitons, because isolated half-quantized vortices can topologically exist only in the D_4BN state and thus splitting into two half-quantized vortices is possible only inside the D_4BN order.

In this paper, we investigate proximity effects of two vortex molecules. As explained above, a singly quantized vortex is of the form of a vortex molecule of two half-quantized non-Abelian vortices connected by a single soliton (three solitons) in the absence (presence) of a magnetic field. In the absence of magnetic field, we find that a transition of half-quantized non-Abelian vortex cores occurs from a ferromagnetic order (connected by a single soliton) to a cyclic order (connected by three solitons), when two vortex molecules come close to each other with increasing the rotation speed. Furthermore, one of three solitons reconnects to one of the other vortex molecule and bridges the two vortex molecules, forming a "covalent bond." Thus, the four constituent half-quantized vortices are connected by one or two soliton(s) alternately. In the presence of a magnetic field below the critical magnetic field $B < B_c$, we find the same transition from two isolated vortex molecules to a "dimerized molecule" with a covalent bonding of solitons when the two vortex molecules come close to each other with increasing the rotation speed.[3] However, we do not find such phenomena in the D_4BN phase above the critical magnetic field. Instead, we find another type of a transition for the polarization direction of the vortex molecules from one parallel to the separation of the two vortex molecules to the other perpendicular to the separation of the two vortex molecules with increasing the external rotation. Then, we further study three and four vortex molecules. In the D_2BN phase below the critical magnetic field, as in the case of two vortex molecules, we find a transition from isolated vortex

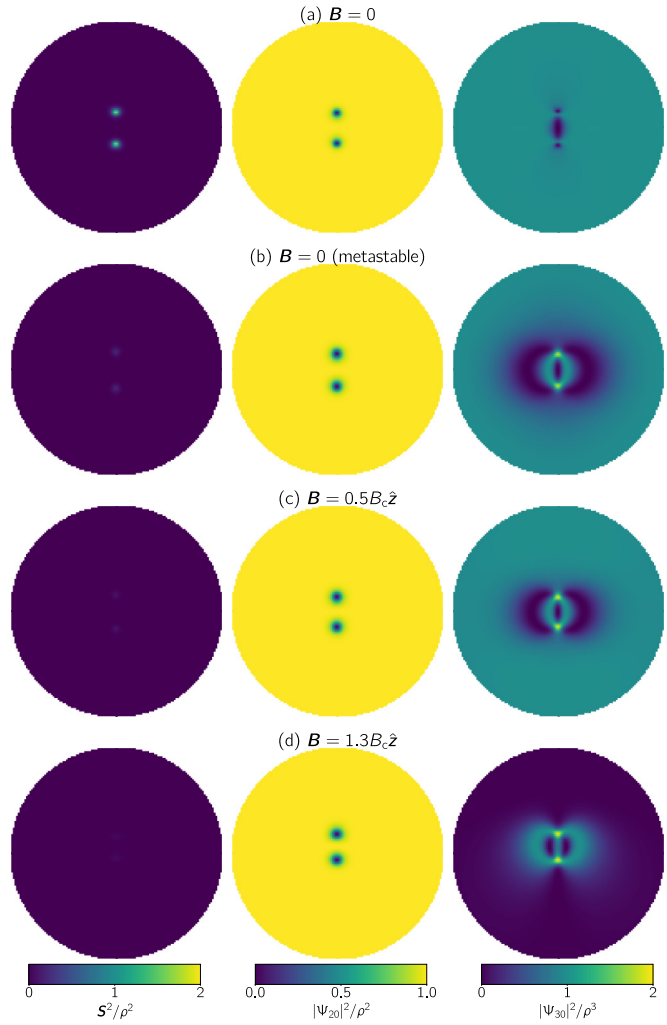

FIG. 1. Singly quantized vortices as molecules of two half-quantized vortices. $\boldsymbol{S}^2$ (left panels), $|\Psi_{20}|^2$ (middle panels), and $|\Psi_{30}|^2$ (right panels) for the single-vortex solution at (a) $T = 0.854T_c$ and $\boldsymbol{B} = 0$, (b) $\boldsymbol{B} = 0.5B_c\hat{z}$, and (c) $\boldsymbol{B} = 1.3B_c\hat{z}$. The radius of the figure shown here is $64p_F/(\pi m_n T_c) \approx 9.29$ pm.

is that constituent half-quantized vortices are *non-Abelian* vortices associated with a non-Abelian first homotopy group.

[3]A similar reconnection of solitons was observed in numerical simulations of two-component BECs [87,92], and similar chemical bonds of vortex molecules were found in multicomponent superconductors with arbitrary charges and Josephson couplings [121].

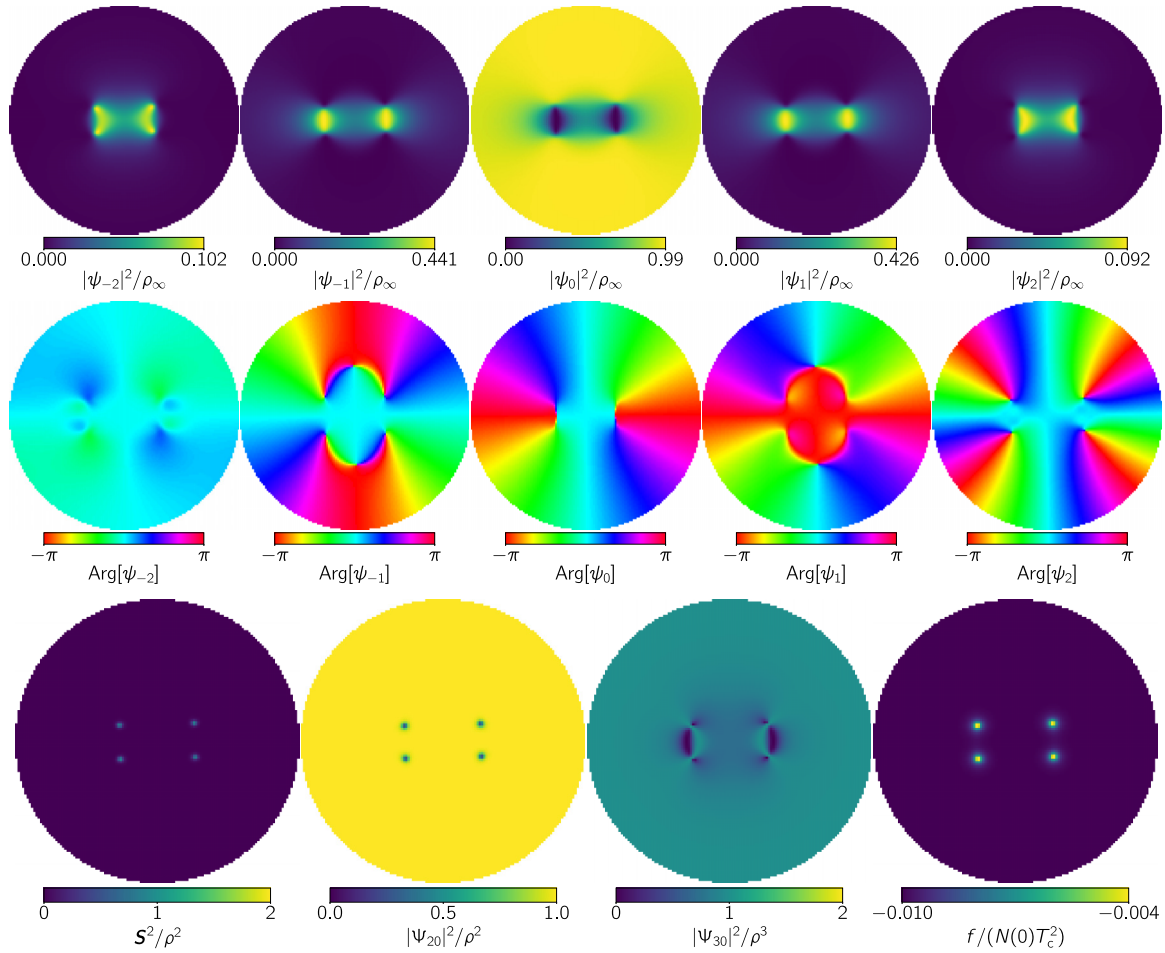

FIG. 2. The most stable two-vortex molecule state in the UN phase at $\boldsymbol{B} = 0$ and $\Omega^2 = 0.8\Omega_0^2$ with $\Omega_0 = 160\pi^2 m_n T_c^2/(256^2 p_F^2) \approx 7.15 \times 10^{15}$ rad fs^{-1}. The squared modulus $|\psi_m|^2$ (top row), argument $\mathrm{Arg}[\psi_m]$ (middle row) of the order parameter, the U(1) × SO(3) invariants S^2, $|\Psi_{20}|^2$, and $|\Psi_{30}|^2$, and the free-energy density f (bottom row) are shown. The radius of the figure shown here is $64 p_F/(\pi m_n T_c) \approx 9.29$ pm.

molecules to trimerized and tetramerized vortex molecules consisting of six and eight half-quantized non-Abelian vortices. In the end of the paper, we also discuss states with many vortex molecules as candidates for neutron star interiors. Unlike singlet-paring superfluids, vortex configuration becomes irregular due to polymerization of vortex molecules or a frustration between spatial configuration and the alignment of vortex molecules.

This paper is organized as follows. In Sec. II, we begin with formulations of $^3P_2$ superfluids within the GL approach in our notation, and shortly summarize our previous results for a single vortex molecule state. In Sec. III, we show our main results for two, three, four, and many vortex molecule states. Section IV is devoted to a summary and discussion.

II. GINZBURG-LANDAU FREE ENERGY AND SINGLE-VORTEX MOLECULE STATE FOR $^3P_2$ NEUTRON SUPERFLUIDS

We start from a brief review of the GL theory for $^3P_2$ superfluids [55] reformulated in the notation of Ref. [56] and single-vortex molecule state within the GL formalism. The details were discussed in Refs. [55,56] for GL theory and Ref. [80] for single-vortex state.

A. Ginzburg-Landau theory

The effective GL Lagrangian density f is given by

$$f = K_0\left(f_{202}^{(0)} + f_{202}^{(1)}\right) + \alpha f_{002} + \beta_0 f_{004} + \gamma_0 f_{006} + \delta_0 f_{008} + \beta_2 f_{022} + \gamma_2 f_{024} + \sum_{4l+2m+n=10} \mathcal{O}(\nabla^l |\boldsymbol{B}|^m A^n), \tag{1}$$

where f_{lmn} is the free energy part including l spatial derivatives ∇, mth order of the magnetic field $\boldsymbol{B}$, and nth order of spin-2 spinor order parameter $\psi = (\psi_2, \psi_1, \psi_0, \psi_{-1}, \psi_{-2})^T$. The spatial derivative term f_{202} is further separated into current-spin independent and dependent parts $f_{202}^{(0)}$ and $f_{202}^{(1)}$, respectively. Each term can be written as

$$f_{202}^{(0)} = 3\boldsymbol{j}^\dagger \cdot \boldsymbol{j},$$

$$f_{202}^{(1)} = 4\boldsymbol{j}^\dagger \cdot \boldsymbol{j} - \frac{i}{2}\boldsymbol{j}^\dagger \cdot \hat{\boldsymbol{S}} \times \boldsymbol{j} - (\boldsymbol{j}^\dagger \cdot \hat{\boldsymbol{S}})(\hat{\boldsymbol{S}} \cdot \boldsymbol{j}),$$

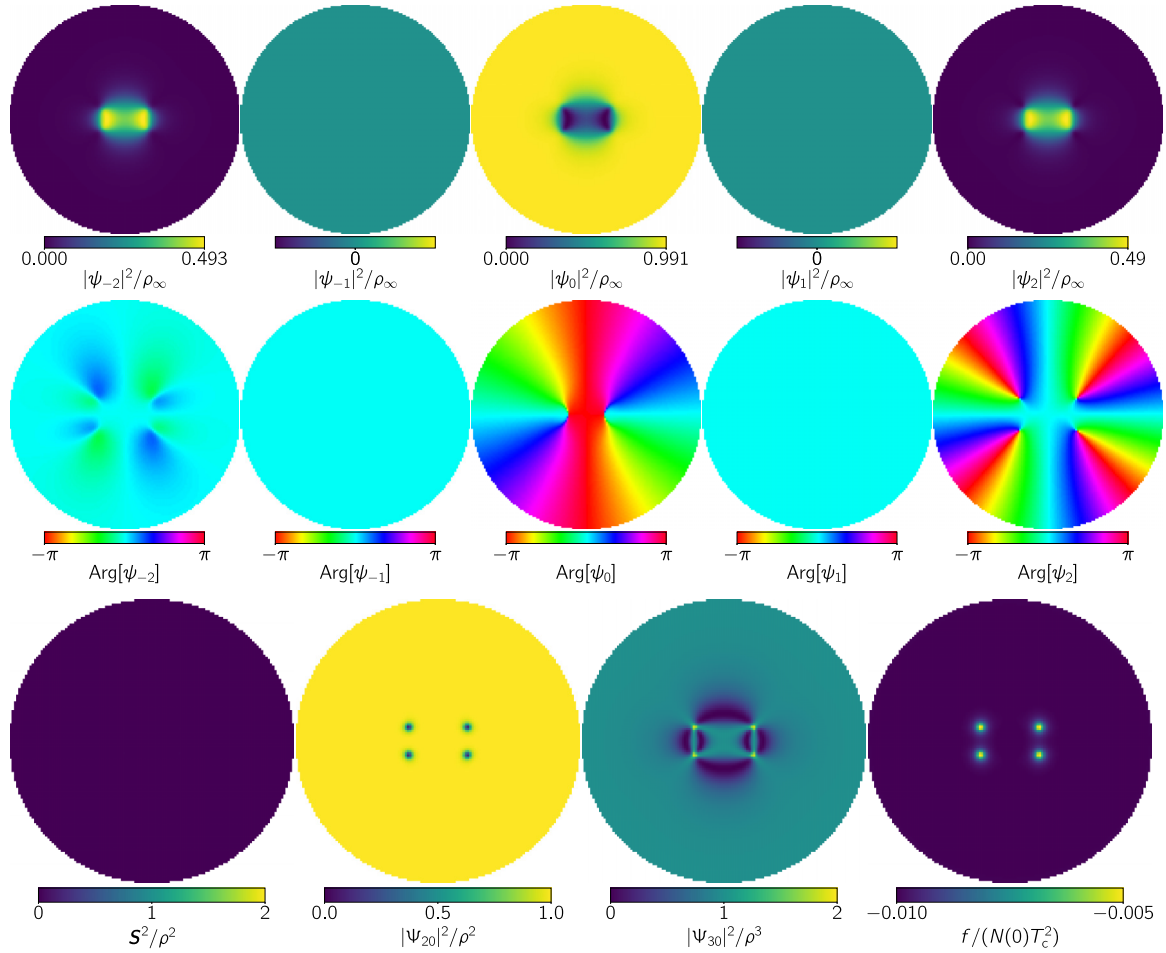

FIG. 3. The most stable two-vortex molecule state in the UN phase at $\boldsymbol{B} = 0$ and $\Omega^2 = 1.0\Omega_0^2$. The squared modulus $|\psi_m|^2$ (top row), argument $\mathrm{Arg}[\psi_m]$ (middle row) of the order parameter, the U(1) × SO(3) invariants S^2, $|\Psi_{20}|^2$, and $|\Psi_{30}|^2$, and the free-energy density f (bottom row) are shown. The radius of the figure shown here is $64p_{\mathrm{F}}/(\pi m_{\mathrm{n}} T_{\mathrm{c}}) \approx 9.29$ pm. The two vortex molecules share two solitons.

$$
\begin{aligned}
f_{002} &= 3\rho, \quad f_{004} = 6\rho^2 + \frac{3}{4}\boldsymbol{S}^2 - \frac{3}{2}|\Psi_{20}|^2, \\
f_{022} &= 2\rho\boldsymbol{B}^2 - \frac{1}{2}\psi^\dagger \hat{S}_{\boldsymbol{B}} \hat{S}_{\boldsymbol{B}} \psi, \\
f_{006} &= -324\rho^3 - 81\rho\boldsymbol{S}^2 + 162\rho|\Psi_{20}|^2 \\
&\quad + 15|\Psi_{30}|^2 - 27|\Phi_{30}|^2, \\
f_{024} &= \left(-106\rho^2 + \frac{9}{2}\boldsymbol{S}^2 + 31|\Psi_{20}|^2 \right)\boldsymbol{B}^2 \\
&\quad + \left(22\rho\psi^\dagger \hat{S}_{\boldsymbol{B}} \hat{S}_{\boldsymbol{B}} \psi + \mathrm{Re}\left[\Psi_{20}^* \psi^T \hat{S}_{\boldsymbol{B}}^T \hat{T} \hat{S}_{\boldsymbol{B}} \psi \right] \right. \\
&\quad \left. + \frac{5}{4}\Psi_{22}^\dagger \hat{S}_{\boldsymbol{B}} \hat{S}_{\boldsymbol{B}} \Psi_{22} + \frac{1}{2}\Phi_{22}^T \hat{S}_{\boldsymbol{B}}^T \hat{T} \hat{S}_{\boldsymbol{B}} \Phi_{22} \right), \\
f_{008} &= 6480\rho^4 + 1944\rho^2\boldsymbol{S}^2 - 5184\rho^2|\Psi_{20}|^2 - 864\rho|\Psi_{30}|^2 \\
&\quad + 2592\rho|\Phi_{30}|^2 + 81\boldsymbol{S}^4 + 648|\Psi_{20}|^4 - 1296\Gamma_4. \quad (2)
\end{aligned}
$$

Here, $\hat{S}_i$ $(i = x, y, z)$ are 5×5 spin-2 matrices,

$$
\boldsymbol{j} \equiv -i\nabla\psi, \quad (3)
$$

and the invariants are given by

$$
\begin{aligned}
&\rho \equiv \psi^\dagger\psi, \quad \boldsymbol{S} \equiv \psi^\dagger \hat{\boldsymbol{S}} \psi, \\
&\Gamma_4 \equiv \mathrm{Re}\left[\Psi_{20}\Phi_{30}^{*2}\right], \quad \Psi_{20} \equiv \sqrt{5} C^{00}_{2m_1,2m_2} \psi_{m_1}\psi_{m_2}, \\
&\Psi_{30} \equiv -\sqrt{\frac{35}{2}} C^{00}_{JM,2m_3} C^{JM}_{2m_1,2m_2} \psi_{m_1}\psi_{m_2}\psi_{m_3}, \\
&\Phi_{30} \equiv -\sqrt{\frac{35}{2}} C^{00}_{JM,2m_3} C^{JM}_{2m_1,2m_2} \psi_{m_1}\psi_{m_2}(-1)^{m_3}\psi^*_{-m_3}, \quad (4)
\end{aligned}
$$

where we have taken the Einstein summation notation for $-2 \leqslant m_{1,2,3} \leqslant 2$, $0 \leqslant J \leqslant 4$, and $-J \leqslant M \leqslant J$ for Ψ_{20}, Ψ_{30}, and Φ_{30} with the Clebsch-Gordan coefficients $C^{JM}_{s_1m_1,s_2m_2}$.

The GL coefficients can be obtained in the weak coupling limit within the quasiclassical approximation starting from the nonrelativistic spin-1/2 fermion field theory as [55]

$$
\begin{aligned}
K_0 &= \frac{7\zeta(3)N(0)p_{\mathrm{F}}^4}{240\pi^2 m_{\mathrm{n}}^2 T^2}, \quad \alpha = \frac{N(0)p_{\mathrm{F}}^2}{3}\log\frac{T}{T_{\mathrm{c}}}, \\
\beta_0 &= \frac{7\zeta(3)N(0)p_{\mathrm{F}}^4}{60\pi^2 T^2}, \quad \gamma_0 = \frac{31\zeta(5)N(0)p_{\mathrm{F}}^6}{13440\pi^4 T^4},
\end{aligned}
$$

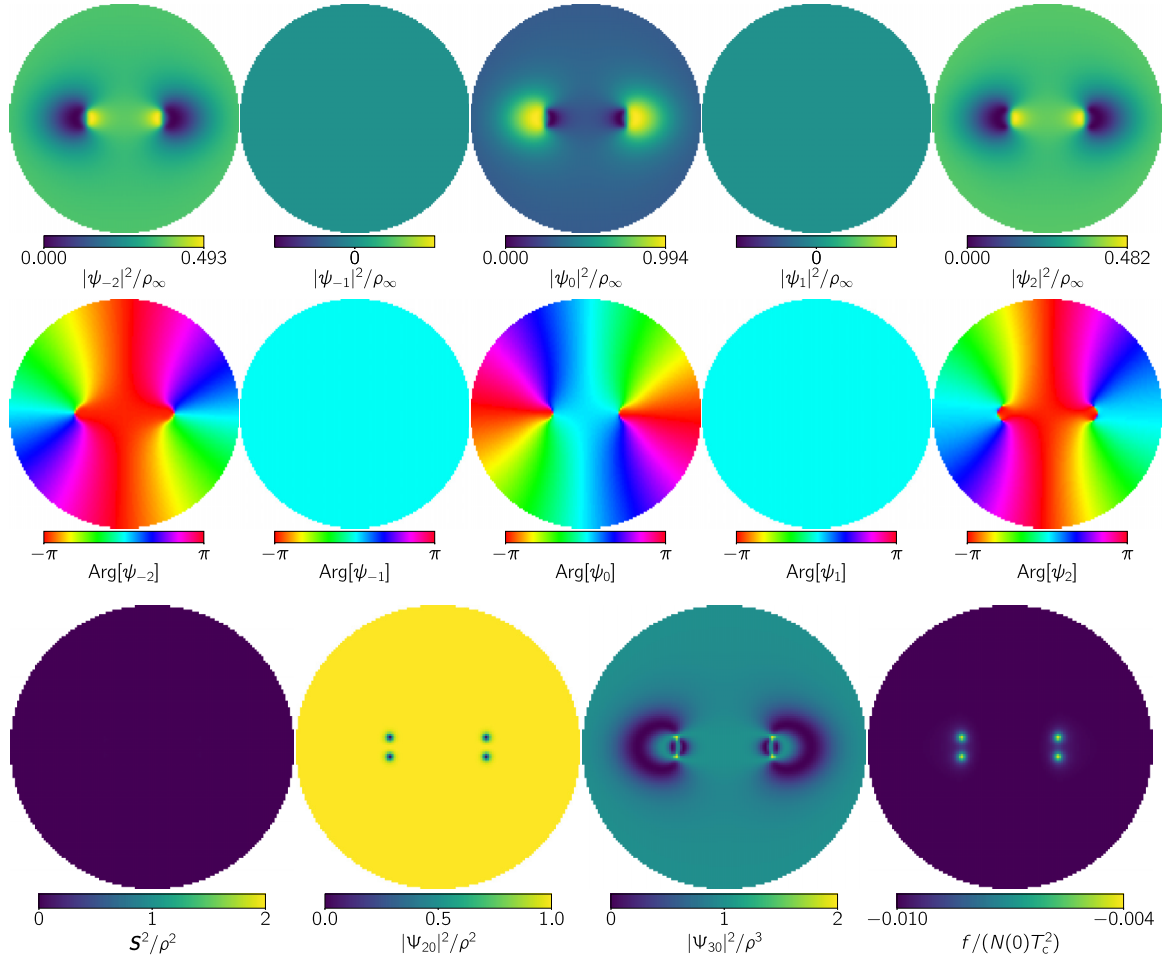

FIG. 4. The metastable two-vortex molecule state in the UN phase at $\boldsymbol{B} = 0$ and $\Omega^2 = 0.8\Omega_0^2$. The squared modulus $|\psi_m|^2$ (top row), argument $\mathrm{Arg}[\psi_m]$ (middle row) of the order parameter, the U(1) × SO(3) invariants S^2, $|\Psi_{20}|^2$, and $|\Psi_{30}|^2$, and the free-energy density f (bottom row) are shown. The radius of the figure shown here is $64p_\mathrm{F}/(\pi m_\mathrm{n} T_\mathrm{c}) \approx 9.29$ pm.

$$\delta_0 = \frac{127\zeta(7)N(0)p_\mathrm{F}^8}{387072\pi^6 T^6}, \quad \beta_2 = \frac{7\zeta(3)N(0)p_\mathrm{F}^2\gamma_\mathrm{n}^2}{48\left(1+F_0^a\right)^2\pi^2T^2},$$
$$\gamma_2 = \frac{31\zeta(5)N(0)p_\mathrm{F}^4\gamma_\mathrm{n}^2}{3840\left(1+F_0^a\right)^2\pi^4T^4} \tag{5}$$

with the temperature T, the critical temperature T_c, the neutron mass m_n, the neutron gyromagnetic ratio γ_n, the Fermi momentum p_F, the state-number density $N(0) = m_\mathrm{n}p_\mathrm{F}/(2\pi)^2$ at the Fermi surface, and the Landau parameter F_0^a. All uniform states were classified in Ref. [56]. The five characteristic symmetric states are ferromagnetic (F), uniaxial nematic (UN), D_4 biaxial nematic (BN), D_2BN, and cyclic (C) states. Each uniform state is characterized by U(1) × SO(3) invariants S^2, $|\Psi_{20}|^2$, and $|\Psi_{30}|^2$ as summarized in Table II.

For the effective Lagrangian density f in Eq. (1), the UN, D_2BN, and D_4BN states are predicted to be realized as the ground states of $^3P_2$ superfluids at $|\boldsymbol{B}| = 0$, $0 < |\boldsymbol{B}| < B_\mathrm{c}$, and $|\boldsymbol{B}| > B_\mathrm{c}$, respectively [73], as summarized in Table I(a). The critical magnetic field B_c separating the D_2BN and D_4BN states depends on the temperature and takes the maximum value $B_\mathrm{c} = 7.06 \times 10^{-2}\pi(1+F_0^a)T_\mathrm{c}/\gamma_\mathrm{n}$ at $T \simeq 0.854T_\mathrm{c}$. With an estimation for the critical temperature $T_\mathrm{c} \approx 0.2$ MeV and the Landau parameter $F_0^a \approx 1$, this critical magnetic field can be estimated as $B_\mathrm{c} \approx 7.36 \times 10^{15}$ G. At $T \lesssim 0.796T_\mathrm{c}$, we obtain $B_\mathrm{c} = 0$.

B. Single vortex molecule solutions

Here, we briefly summarize our previous results [80] for singly quantized vortex states as molecules of two half-quantized vortices.

First, we consider the ansatz for vortex solutions with vortex cores placed at $r = 0$ in the cylindrical coordinates (r, θ, z) and the boundary $\psi_{r\to\infty}$ far from vortex cores. For singly quantized vortices, the order parameters behave as $\psi_{-2\leqslant m\leqslant 2}|_{r\to\infty} \propto e^{i\theta}$. For $\boldsymbol{B} = 0$, the uniform ground state is degenerate within the possible UN state

$$\psi_{\pm2} = \frac{e^{i\phi\mp 2a}\sqrt{3}\sin^2 b}{2\sqrt{2\rho}}, \quad \psi_{\pm1} = \frac{e^{i\phi\mp a}\sin(2b)}{2\sqrt{2\rho}},$$
$$\psi_0 = \frac{e^{i\phi}\{1+3\cos(2b)\}}{4\sqrt{\rho}}, \tag{6}$$

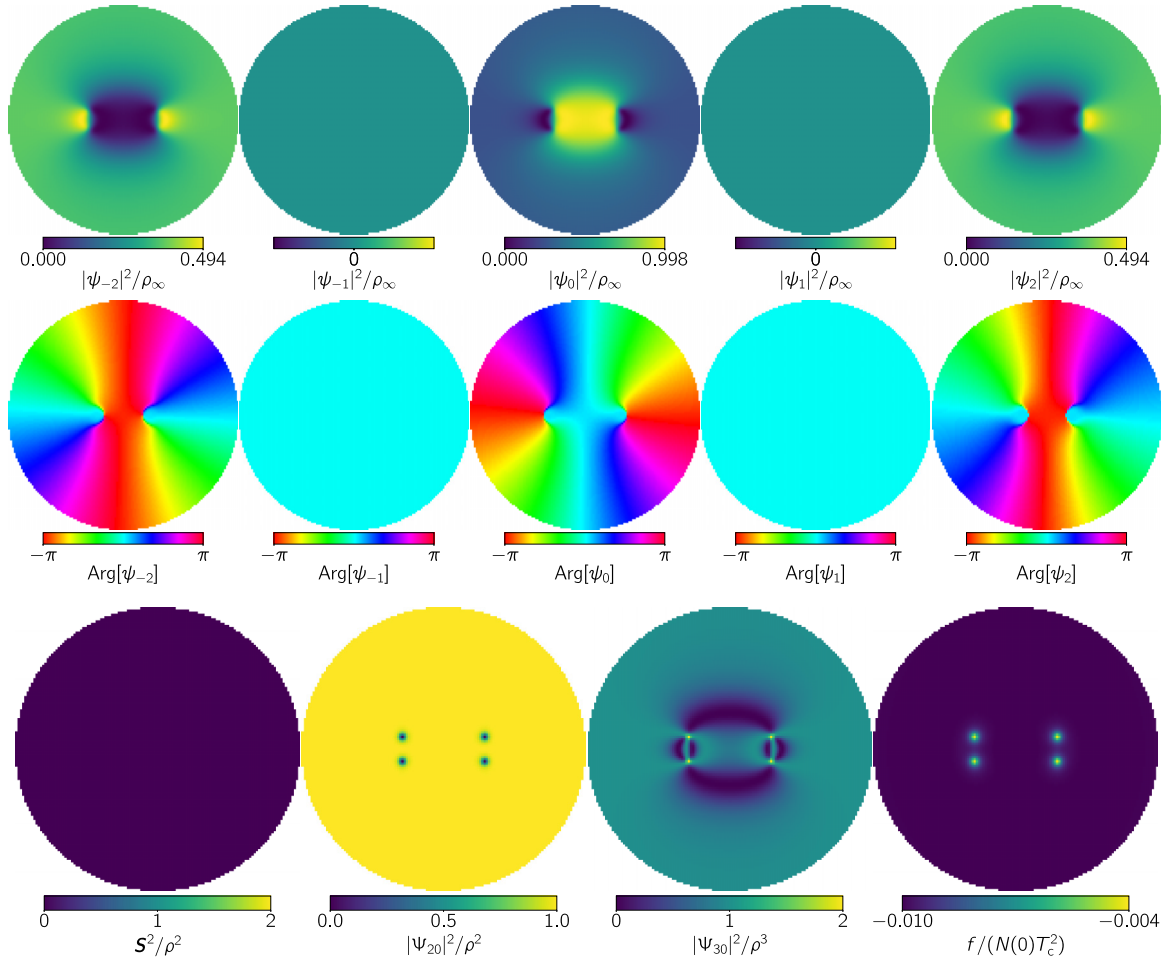

FIG. 5. The metastable two-vortex molecule state in the UN phase at $\boldsymbol{B} = 0$ and $\Omega^2 = 1.0\Omega_0^2$. The squared modulus $|\psi_m|^2$ (top row), argument $\mathrm{Arg}[\psi_m]$ (middle row) of the order parameter, the U(1) × SO(3) invariants S^2, $|\Psi_{20}|^2$, and $|\Psi_{30}|^2$, and the free-energy density f (bottom row) are shown. The radius of the figure shown here is $64p_F/(\pi m_n T_c) \approx 9.29$ pm.

for $0 \leqslant a, 2b, \phi < 2\pi$. Here, a, b, and ϕ represent overall spin rotations along the z and y axes, and overall phase shift, respectively. Under the spatial phase gradient $e^{i\theta}$ for the vortex solution, the current-spin dependent free energy density $f_{202}^{(2)}$ in Eq. (1) favors $b = 0$ giving

$$\psi \xrightarrow{r\to\infty} \frac{e^{i\theta}}{\sqrt{\rho}}(0, 0, 1, 0, 0)^T. \tag{7}$$

In the case of $0 < |\boldsymbol{B}| < B_c$, we obtain

$$\psi \xrightarrow{r\to\infty} \frac{e^{i\theta}}{\sqrt{\rho}}\left(\frac{e^{-2ia}\sin g}{\sqrt{2}}, 0, \cos g, 0, \frac{e^{2ia}\sin g}{\sqrt{2}}\right)^T, \tag{8}$$

where g depends on $|\boldsymbol{B}|$ and satisfies $\pi/3 < g < \pi/2$, making $\psi|_{r\to\infty}$ to be the D_2BN state. a also represents the overall spin rotation along the z axis and takes arbitrary (fixed) value without (with) the current-spin dependent free energy $f_{202}^{(1)}$. In the limit of $|\boldsymbol{B}| \searrow 0$, g becomes $g \to \pi/3$ giving

$$\psi \xrightarrow{r\to\infty} \frac{e^{i\theta}}{\sqrt{\rho}}\left(\frac{e^{-2ia}\sqrt{3}}{2\sqrt{2}}, 0, \frac{1}{2}, 0, \frac{e^{2ia}\sqrt{3}}{2\sqrt{2}}\right)^T. \tag{9}$$

This solution belongs to the UN state in Eq. (6) with $b = \pi/2$, but is different from that for $\boldsymbol{B} = 0$ shown in Eq. (7), which leads the discontinuity between $\boldsymbol{B} = 0$ and $|\boldsymbol{B}| \searrow 0$ and the metastable solution at $\boldsymbol{B} = 0$. For the case of $|\boldsymbol{B}| \geqslant B_c$, g becomes $g = \pi/2$, giving

$$\psi \xrightarrow{r\to\infty} \frac{e^{i\theta}}{\sqrt{\rho}}\left(\frac{e^{-2ia}}{\sqrt{2}}, 0, 0, 0, \frac{e^{2ia}}{\sqrt{2}}\right)^T, \tag{10}$$

which belongs to the D_4BN state.

Next, we show our numerical results for singly quantized vortex solutions. They are obtained by minimizing the free-energy density f under the boundary conditions with the cylindrical coordinates (r, θ, z):

$$\psi_m(\theta + \pi)|_{r=L} = -\psi_m(\theta)|_{r=L}, \tag{11}$$

at the boundary $r = L$, which induces a singly quantized vortex solution. The minimization of the free energy density f can be done by finding the stationary solution of the GL equation

$$\frac{\delta f}{\delta \psi_m^*} = 0. \tag{12}$$

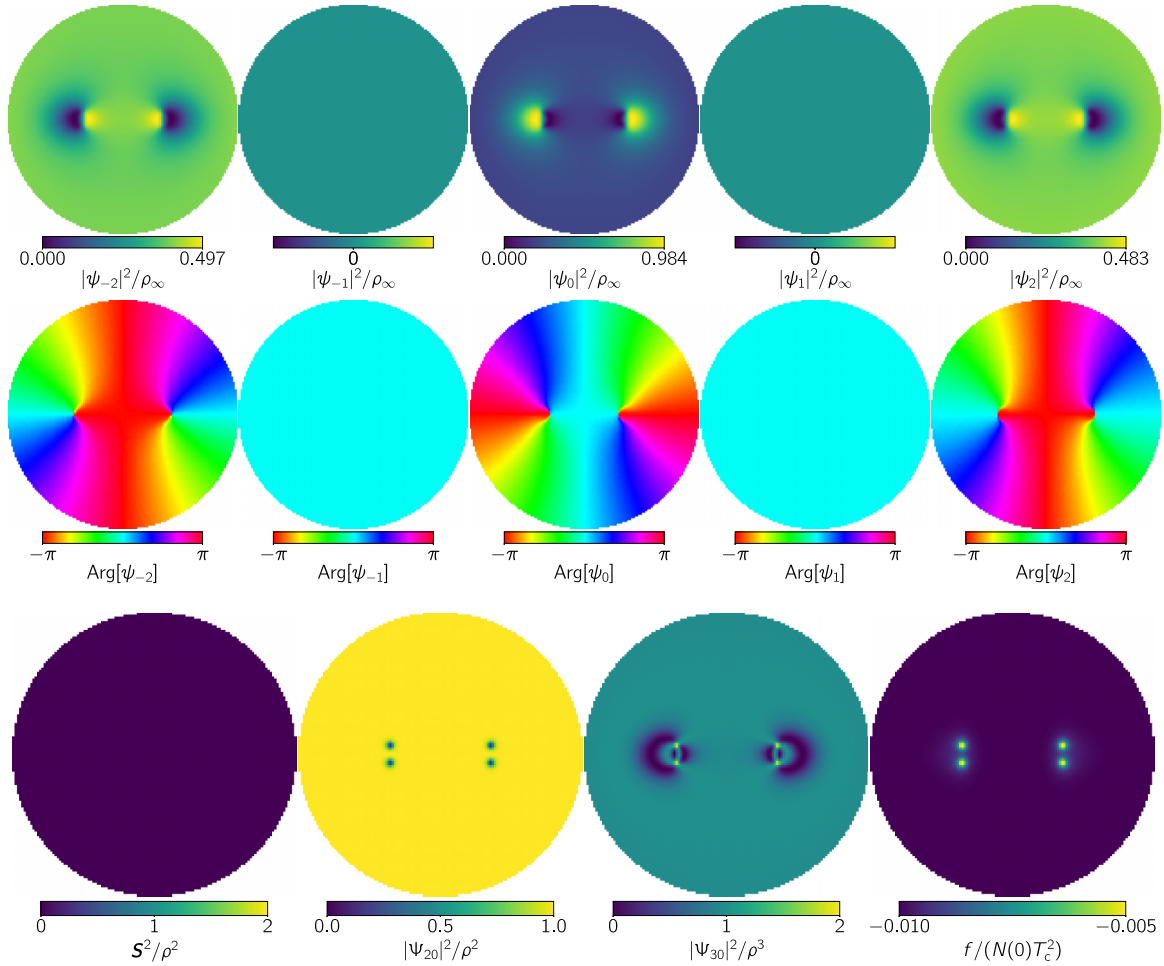

FIG. 6. The two-vortex molecule state in the D_2BN phase at $\boldsymbol{B} = 0.5B_c\hat{\boldsymbol{z}}$ and $\Omega^2 = 0.8\Omega_0^2$. The squared modulus $|\psi_m|^2$ (top row), argument $\mathrm{Arg}[\psi_m]$ (middle row) of the order parameter, the U(1) × SO(3) invariants S^2, $|\Psi_{20}|^2$, and $|\Psi_{30}|^2$, and the free-energy density f (bottom row) are shown. The radius of the figure shown here is $64p_F/(\pi m_n T_c) \approx 9.29$ pm.

The solution of Eq. (12) can be obtained by the Nesterov's method with introducing the relaxation time t and the dependence of the order parameter ψ_m. The time dependences of ψ_m is given by

$$\ddot{\psi}_m = -\frac{\delta f}{\delta \psi_m^*} - \frac{3}{t}\dot{\psi}_m, \quad \dot{\psi}_m(t=0) = 0. \tag{13}$$

After the long time evolution of Eq. (13), we obtain the solution of Eq. (12). We note that Eq. (13) is just one of methods to effectively obtain solutions to Eq. (12).

Figure 1 shows numerical solutions [80] at the temperature $T = 0.854T_c$ and the magnetic field $\boldsymbol{B} = 0, 0.5B_c\hat{\boldsymbol{z}}$, and $1.3B_c\hat{\boldsymbol{z}}$. In any cases, a singly quantized vortex splits into two half-quantized vortices with holes of $|\Psi_{20}|^2$ forming a vortex molecule. The fact that isolated half-quantized vortices can topologically exist only in the D_4BN state implies that the D_4BN order should appear around the vortex core for even for $|\boldsymbol{B}| < B_c$ in which the ground states are either UN or D_2BN states [Figs. 1(a)–1(c)]. In fact, we can confirm that the D_4BN order characterized by $S^2 = 0$, $|\Psi_{20}|^2/\rho^2 = 1$, and $|\Psi_{30}|^2/\rho^3 = 0$ appears as one (three) soliton(s) bridging two vortex cores for Fig. 1(a) at $\boldsymbol{B} = 0$ [Fig. 1(b) at $\boldsymbol{B} = 0$ and Fig. 1(c) at $\boldsymbol{B} = 0.5B_c\hat{\boldsymbol{z}}$], as can be seen in the plot of $|\Psi_{30}|^2$ locally inducing the D_4BN order. At $\boldsymbol{B} = 1.3B_c\hat{\boldsymbol{z}}$ shown in Fig. 1(d), where D_4BN state becomes the ground state, two half-quantized vortices also form a vortex molecule bridged by three D_2BN solitons characterized by $0 < |\Psi_{30}|^2/\rho^3 < 1$. The cores of the half-quantized vortices are filled by F, C, C, and C orders for Figs. 1(a), 1(b), 1(c), and 1(d), respectively. At the numerical boundary $r = L$, the order parameters for Figs. 1(a), 1(b), 1(c), and 1(d) satisfy Eqs. (7), (9), (8), and (10), respectively. In particular, the two solutions at $\boldsymbol{B} = 0$ shown in Figs. 1(a) and 1(b) correspond to the most stable and metastable ones, respectively, and the latter was missing in the previous study [80].

III. MULTIVORTEX STATE FOR $^3P_2$ NEUTRON SUPERFLUIDS

In this section, we show our main results for multivortex state for $^3P_2$ superfluids. Because two vortices with the same circulation have long-range repulsion, they cannot be

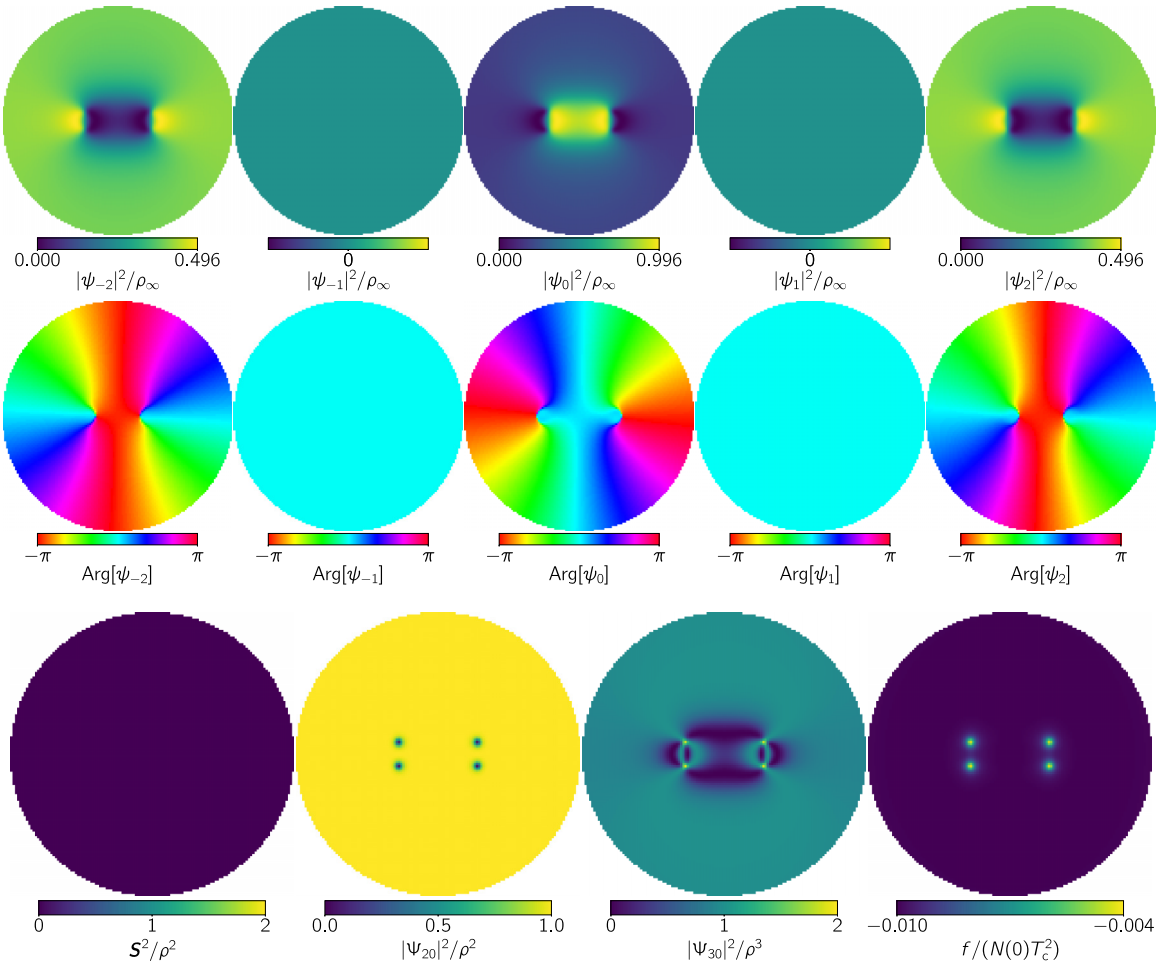

FIG. 7. The two-vortex molecule state in the D_2BN phase at $\boldsymbol{B} = 0.5B_c\hat{\boldsymbol{z}}$ and $\Omega^2 = 1.0\Omega_0^2$. The squared modulus $|\psi_m|^2$ (top row), argument $\mathrm{Arg}[\psi_m]$ (middle row) of the order parameter, the U(1) × SO(3) invariants S^2, $|\Psi_{20}|^2$, and $|\Psi_{30}|^2$, and the free-energy density f (bottom row) are shown. The radius of the figure shown here is $64p_F/(\pi m_n T_c) \approx 9.29$ pm.

stabilized by the boundary condition such as Eq. (11). We thus introduce an external rotation term by rewriting the free-energy density f as $f - \mathrm{Re}[\boldsymbol{\Omega}\cdot\boldsymbol{L}]$ [84], where $\boldsymbol{\Omega} = (0, 0, \Omega)$ is the rotation vector parallel to the z axis, and $\boldsymbol{L} = m_n^2 p_F \psi^\dagger(-i\boldsymbol{r}\times\nabla)\psi$ is the angular momentum. This is nothing but a physical situation realized in rotating neutron stars. As well as the case of the single-vortex solutions, we obtain the stationary solution of the GL equation by the Nesterov's method in Eq. (13) under the boundary condition

$$(\nabla\psi)_\parallel|_{r=L} = 0, \tag{14}$$

where $(\,)_\parallel$ means the component parallel to $\hat{\boldsymbol{r}}$ in the cylindrical coordinate, and L is the numerical boundary set to be $L = 128p_F/(\pi m_n T_c) \approx 18.6$ pm.

A. Two-vortex molecule states

1. The stable solution in the case of zero magnetic field $B = 0$

For the $\boldsymbol{B} = 0$ case in which the UN phase is the ground state, we expect the F-core vortex molecules connected by a single D_4BN soliton as shown in Fig. 1(a). Figure 2 shows the two-vortex molecule state at $\boldsymbol{B} = 0$ and $\Omega^2 = 0.8\Omega_0^2$, where Ω_0 is defined as $\Omega_0 = 160\pi^2 m_n T_c^2/(256^2 p_F^2) \approx 7.30$ rad fs^{-1}. Compared to the singly quantized vortex state, the two D_4BN solitons between half-quantized vortex cores repel each other to bend, as can be clearly seen in $|\Psi_{30}|^2$. At the boundary $r = L$, the order parameter approximately satisfies

$$\psi|_{r=L} = \frac{e^{2i\theta}}{\sqrt{\rho}}(0, 0, 1, 0, 0)^T, \tag{15}$$

which is just the double winding of the singly quantized vortex solution Eq. (7) at $\boldsymbol{B} = 0$.

With increasing the rotation, the "dimerization" of two vortex molecules occurs while keeping the boundary state unchanged as shown in Eq. (15). Figure 3 shows the two-vortex molecule state consisting of four half-quantized vortices at $\Omega^2 = 1.0\Omega_0^2$. The details of the dimerization is as follows. First, the F-core vortex molecules having one D_4BN soliton changes to C-core vortex molecules having three D_4BN solitons as in the case of the vortex molecule at $0 < |\boldsymbol{B}| < B_c$.

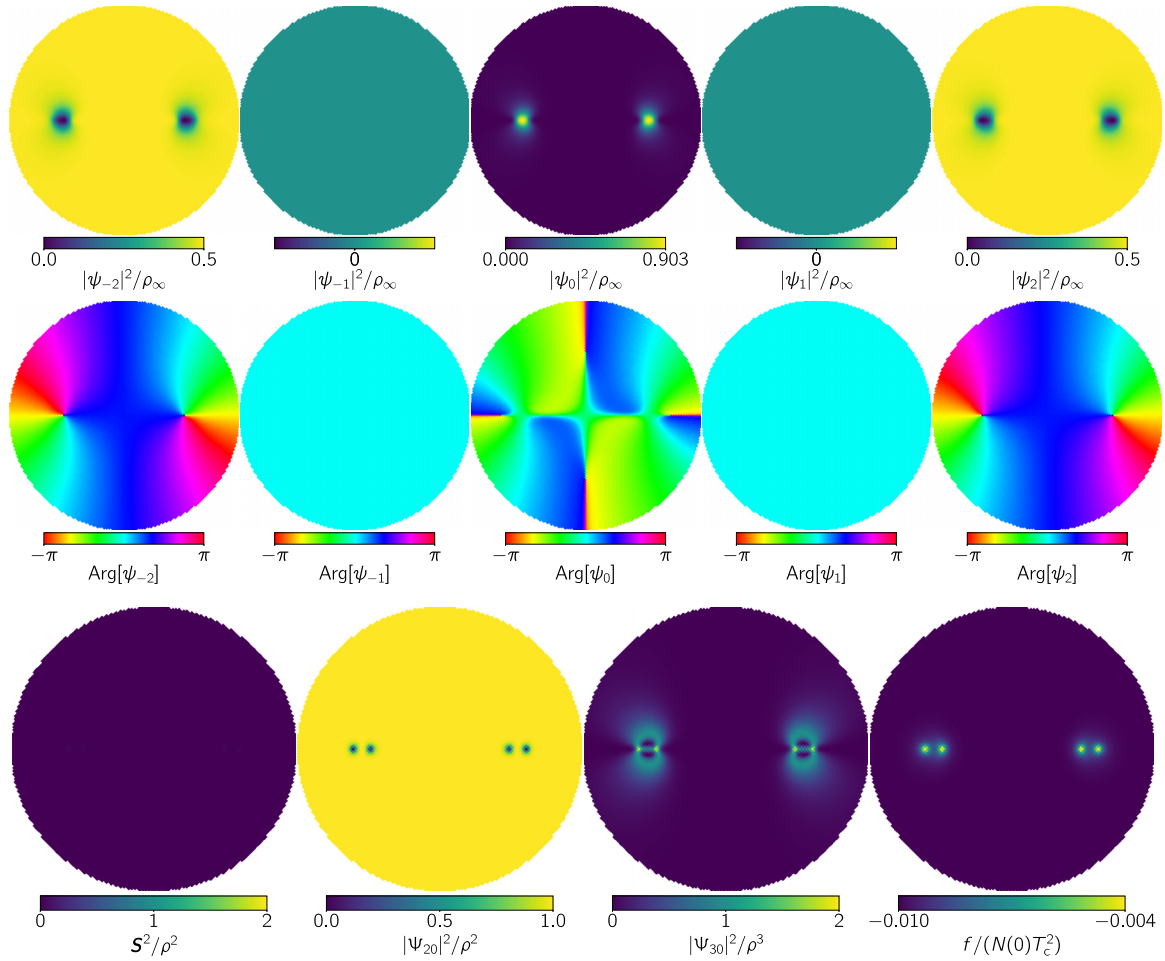

FIG. 8. The two-vortex molecule state in the D_4BN phase at $\boldsymbol{B} = 1.3B_c\hat{\boldsymbol{z}}$ and $\Omega^2 = 0.4\Omega_0^2$. The squared modulus $|\psi_m|^2$ (top row), argument $\mathrm{Arg}[\psi_m]$ (middle row) of the order parameter, the U(1) × SO(3) invariants $\boldsymbol{S}^2$, $|\Psi_{20}|^2$, and $|\Psi_{30}|^2$, and the free-energy density f (bottom row) are shown. The radius of the figure shown here is $64p_{\mathrm{F}}/(\pi m_{\mathrm{n}} T_{\mathrm{c}}) \approx 9.29$ pm.

Then, one of three D_4BN solitons reconnect to one of the other molecules to be shared by the two vortex molecules to form a "covalent bond". In Fig. 3, the upper and lower D_4BN solitons in $|\Psi_{30}|^2$ are covalent bonds between left and right vortex molecules. The transition from the two isolated F-core vortex molecules to a dimerized C-core vortex molecule occurs at $\Omega^2 \simeq \Omega_0^2$.

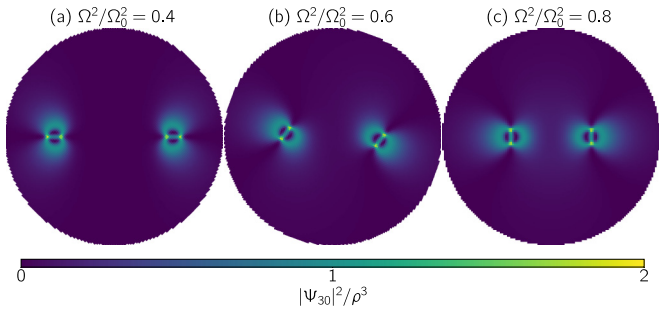

FIG. 9. A transition of the polarization direction of the two-vortex molecules in the D_4BN phase. $|\Psi_{30}|^2$ for two-vortex state in the D_4BN phase at $\boldsymbol{B} = 1.3B_c\hat{\boldsymbol{z}}$ and (a) $\Omega^2 = 0.4\Omega_0^2$, (b) $\Omega^2 = 0.6\Omega_0^2$, and (c) $\Omega^2 = 0.8\Omega_0^2$. The radius of the figure shown here is $64p_{\mathrm{F}}/(\pi m_{\mathrm{n}} T_{\mathrm{c}}) \approx 9.29$ pm.

2. *The metastable solution in the case of zero magnetic field* $\boldsymbol{B} = \boldsymbol{0}$

As well as singly quantized vortex states, there are metastable solutions having the other boundary

$$\psi|_{r=L} = \frac{e^{2i\theta}}{\sqrt{\rho}}\left(\frac{e^{-2ia}\sqrt{3}}{2\sqrt{2}}, 0, \frac{1}{2}, 0, \frac{e^{2ia}\sqrt{3}}{2\sqrt{2}}\right)^T, \tag{16}$$

which is double winding of Eq. (9). In this case, we expect the C-core vortex molecule connected by three D_4BN solitons as shown in Fig. 1(b). Figure 4 (Fig. 5) shows the metastable two-vortex molecule state at $\boldsymbol{B} = 0$ and $\Omega^2 = 0.8\Omega_0^2$ ($\Omega^2 = 1.0\Omega_0^2$). In Fig. 4, there are two isolated vortex molecules in which the three D_4BN solitons connect half-quantized vortices. Compared to the single vortex state shown in Fig. 1(b), the D_4BN soliton in the side of the other vortex molecule is shorten. On the other hand, the D_4BN soliton in the opposite side is enlarged and bent. As a result, a symmetric structure of one vortex molecule as shown in Fig. 1(b) is strongly distorted.

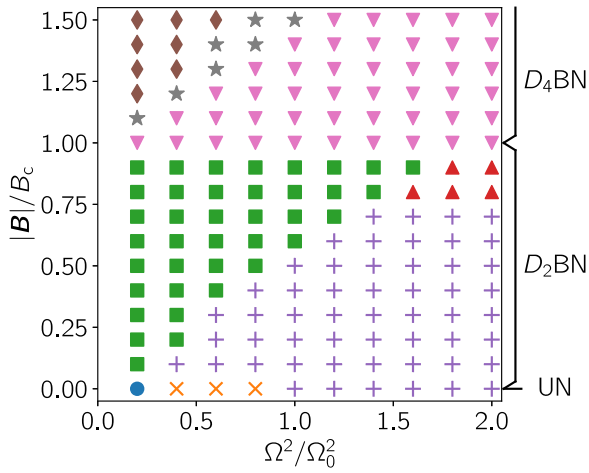

FIG. 10. The Ω–$|\boldsymbol{B}|$ phase diagram for two-vortex molecule states. •: Coexistence of isolated stable F-core molecules and isolated metastable C-core molecules. ×: Coexistence of isolated stable F-core molecules, isolated metastable C-core molecules, dimerized stable molecule, and dimerized metastable molecule. −: Coexistence of isolated metastable C-core molecules, dimerized stable molecule, and dimerized metastable molecule. ■: isolated C-core molecules. +: Coexistence of isolated C-core molecules and dimerized molecule. ▲: Dimerized molecule. ♦: Molecules with $\theta_{\rm molecule} = 0$. ▼: Molecules with $\theta_{\rm molecule} = \pi/2$. ★: Molecules with $0 < \theta_{\rm molecule} < \pi/2$.

As well as the stable case, increasing Ω causes the dimerization of vortex molecules under the same boundary condition Eq. (16). The shape of the dimerized vortex molecule is similar to that shown in Fig. 3, i.e., there are two D_4BN covalent bonds shared by the two vortex molecules.

3. *The case of a small magnetic field* $0 < |\boldsymbol{B}| < B_c$

For the $0 < |\boldsymbol{B}| < B_c$ case in which the D_2BN phase is the ground state, we expect the C-core vortex molecule connected by three D_4BN solitons as shown in Fig. 1(c). Figures 6 (Fig. 7) shows two-vortex molecule state at $\boldsymbol{B} = 0.5B_c\hat{z}$ and $\Omega^2 = 0.8\Omega_0^2$ ($\Omega^2 = 1.0\Omega_0^2$). Two characteristic structures for two isolated vortex molecules shown in Fig. 6 and the dimerized vortex molecule shown in Fig. 7 are almost the same as those for the metastable solutions at $\boldsymbol{B} = 0$ for Figs. 4 and 5, while the order parameter at the boundary satisfy

$$\psi|_{r=L} = \frac{e^{2i\theta}}{\sqrt{\rho}}\left(\frac{e^{-2ia}\sin g}{\sqrt{2}}, 0, \cos g, 0, \frac{e^{2ia}\sin g}{\sqrt{2}}\right)^T, \quad (17)$$

which is double winding of Eq. (8). As well as the singly quantized vortex solution, the two-vortex molecule state in the D_2BN phase at $0 < |\boldsymbol{B}| < B_c$ continuously changes to the metastable state in the UN phase at $\boldsymbol{B} = 0$ [$g \to \pi/3$ limit in Eq. (17) at the boundary].

4. *The case of large magnetic field* $|\boldsymbol{B}| \geqslant B_c$

Finally, for the $|\boldsymbol{B}| \geqslant B_c$ case in which the D_4BN phase is the ground state, we expect the C-core vortex molecule connected by three D_2BN solitons as shown in Fig. 1(c). Figure 8 shows the two-vortex molecule state at $\boldsymbol{B} = 1.3B_c\hat{z}$ and $\Omega^2 = 0.4\Omega_0^2$. There are two isolated vortex molecules in each of which the three D_2BN solitons connect two half-quantized vortices. At the boundary, the order parameter satisfies

$$\psi|_{r=L} = \frac{e^{2i\theta}}{\sqrt{\rho}}\left(\frac{e^{-2ia}}{\sqrt{2}}, 0, 0, 0, \frac{e^{2ia}}{\sqrt{2}}\right)^T, \quad (18)$$

which is double winding of Eq. (10). We define the molecule angle $\theta_{\rm molecule}$ as the angle between the polarization direction of each vortex molecule and the direction of separation of the centers of the two vortex molecules. In Fig. 8, the molecule angle takes $\theta_{\rm rel} = 0$. On the other hand, for the $|\boldsymbol{B}| < B_c$ cases shown in Figs. 2, 3, and 6, the molecule angle takes $\theta_{\rm molecule} = \pi/2$.

Being different from the $|\boldsymbol{B}| < B_c$ cases, the dimerization of vortex molecules never occurs even with increasing the rotation frequency Ω. On the other hand, a rapid change of $\theta_{\rm molecule}$ from 0 to $\pi/2$ occurs. Figure 9 shows $|\Psi_{30}|^2$ profiles for the two-vortex molecule states at the rotation frequencies $\Omega^2/\Omega_0^2 = 0.4$ [panel (a)], 0.6 [panel (b)], and 0.8 [panel (c)], and the molecule angle $\theta_{\rm molecule}$ takes $\theta_{\rm molecule} \approx 0, 0.22\pi$, and $\pi/2$, respectively.

5. *Phase diagram*

Figure 10 shows the $\Omega-|\boldsymbol{B}|$ phase diagram for two-vortex molecule states. The dimerized molecules for $|\boldsymbol{B}| < B_c$ and molecules with $\theta_{\rm molecule} = \pi/2$ can exist at large Ω and small $|\boldsymbol{B}|$. This result supports that these states originate from a proximity effect between two vortex molecules, because the distance between molecules decreases with increasing Ω and the size of a molecule decreases with increasing $|\boldsymbol{B}|$ (see Fig. 5(b) in Ref. [80]). At $|\boldsymbol{B}| < B_c$, the dimerized molecule state coexists with the isolated molecule state in a wide region of the phase diagram (×, −, and + symbols). Here, the coexistence of several states means that one state is stable and others are metastable, or that some states are degenerate and equally stable.

To check this, we calculate the two-dimensional free energy $F = \int d^2x\, f$. Figure 11 shows the two-dimensional free energy F as a function of Ω^2 at $|\boldsymbol{B}| = 0$, where the isolated stable F-core molecule state (see Fig. 2), the isolated metastable C-core molecule state (see Fig. 4), the dimerized stable molecule state (see Fig. 3), and the dimerized metastable molecule state (see Fig. 5) are stabilized. The isolated stable F-core molecule state and dimerized stable molecule state are stable states at small and large rotation frequencies Ω, respectively, having lower free-energy than those of the isolated metastable C-core molecule state and the dimerized metastable molecule state. On the other hand, the isolated stable F-core (metastable C-core) molecule state and the dimerized stable (metastable) molecule state have almost degenerate energies in a wide range of Ω, which does not change in the case of finite values of $|\boldsymbol{B}|$ (+ symbols in Fig. 10).

B. Three and four-vortex molecule states

For more than two vortex molecule states, we expect various stable configurations such as completely isolated molecules, partially polymerized molecules, fully polymer-

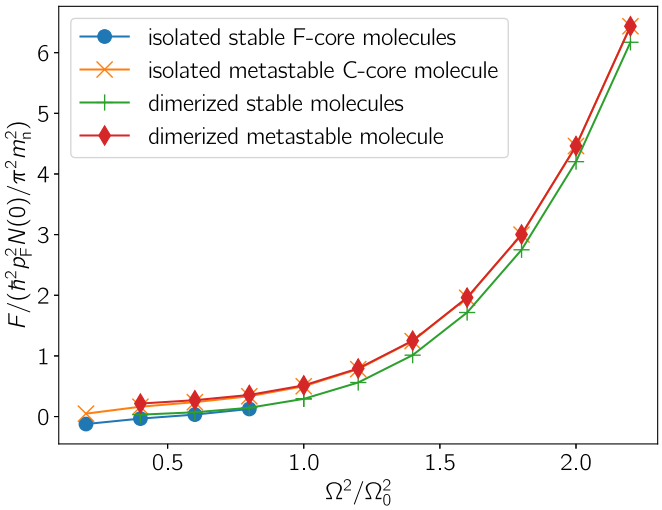

FIG. 11. Two-dimensional free energy $F = \int d^2x\, f$ at $|\boldsymbol{B}| = 0$ as a function of Ω^2 for the isolated stable F-core molecule state, the isolated metastable C-core molecule state, the dimerized stable molecule state, and the dimerized metastable molecule state.

ized molecule at $|\boldsymbol{B}| < B_c$, and clusters of molecule pairs with various θ_{molecule} at $|\boldsymbol{B}| > B_c$. Actually, it is quite difficult to exhaust all (meta)stable states.

Instead, here we just show several characteristic examples for three and four-vortex states. Figure 12 shows six examples of three and four vortex molecule states. At $|\boldsymbol{B}| < B_c$, we have various kinds of "polymerization" of vortex molecules. In Fig. 12(a) and 12(d), we have one dimerized molecule and one isolated molecule, and two dimerized molecules, as three and four vortex molecule states, respectively. We further obtain

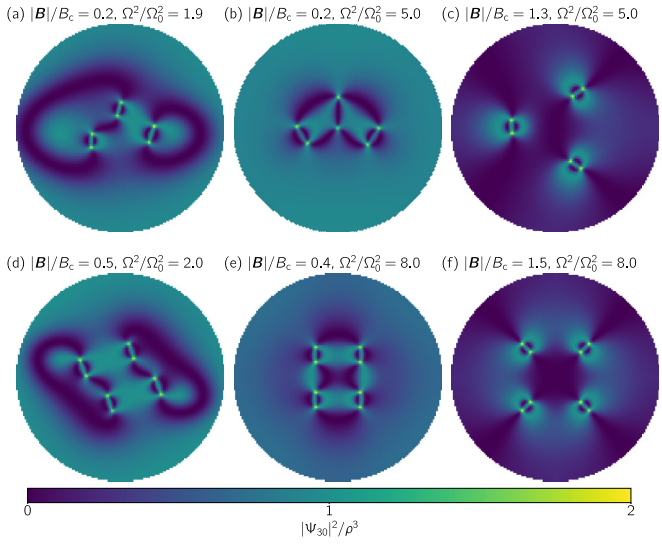

FIG. 12. $|\Psi_{30}|^2$ for three-vortex states (upper panels) and four-vortex states (lower panels) at (a) $\boldsymbol{B} = 0.2B_c\hat{\boldsymbol{z}}$ and $\Omega^2 = 1.9\Omega_0^2$, (b) $\boldsymbol{B} = 0.2B_c\hat{\boldsymbol{z}}$ and $\Omega^2 = 5.0\Omega_0^2$, (c) $\boldsymbol{B} = 1.3B_c\hat{\boldsymbol{z}}$ and $\Omega^2 = 5.0\Omega_0^2$, (d) $\boldsymbol{B} = 0.5B_c\hat{\boldsymbol{z}}$ and $\Omega^2 = 2.0\Omega_0^2$, and (e) $\boldsymbol{B} = 0.4B_c\hat{\boldsymbol{z}}$ and $\Omega^2 = 8.0\Omega_0^2$, and (f) $\boldsymbol{B} = 1.5B_c\hat{\boldsymbol{z}}$ and $\Omega^2 = 8.0\Omega_0^2$. The radius of the figure shown here is $64p_F/(\pi m_n T_c) \approx 9.29$ pm.

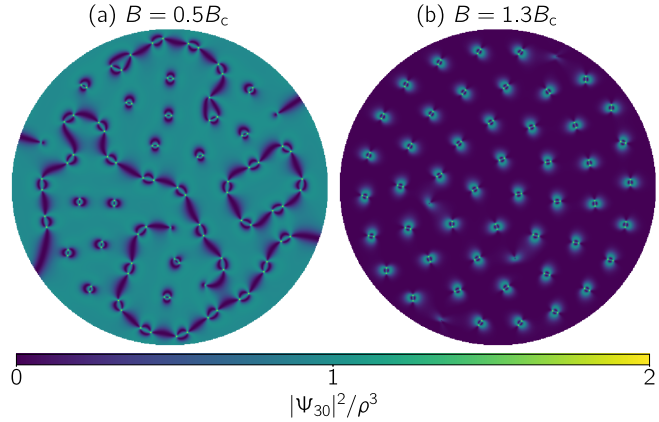

FIG. 13. $|\Psi_{30}|^2$ for states with 50 vortices at (a) $\boldsymbol{B} = 0.5B_c\hat{\boldsymbol{z}}$ and $\Omega^2 = \Omega_0^2$, (c) $\boldsymbol{B} = 1.3B_c\hat{\boldsymbol{z}}$ and $\Omega^2 = \Omega_0^2$. The radius of the figure shown here is $256p_F/(\pi m_n T_c) \approx 37.2$ pm.

"trimerized" and "tetramerized" molecules in Figs. 12(b) and 12(d), respectively. At $|\boldsymbol{B}| \geqslant B_c$, there are also various kinds of clusters of vortex molecules. We show symmetric examples of them in Figs. 12(c) and 12(f).

C. States with many vortex molecules

In the end of the section, we discuss a system with many vortices that can be candidates realized in rotating neutron star interiors. Figure 13 shows systems having 50 vortices in the radius $256p_F/(\pi m_n T_c) \approx 37.2$ pm under the rotation $\Omega = \Omega_0$. In panel (a) for $|\boldsymbol{B}| < B_c$, we obtain a mixture of single vortex molecules and long vortex chains polymerized through covalent bonds between vortex molecules. In panel (b) for $|\boldsymbol{B}| > B_c$, on the other hand, vortex molecules form a lattice structure. However, its structure is irregular and different from the regular triangular configuration that is expected for the vortex lattice in singlet-pairing superfluids. We expect that this irregularity comes from a frustration between the spatial arrangement and internal alignment of vortex molecules. As a consequence, we obtain irregular spatial structures of vortex molecules at both $|\boldsymbol{B}| < B_c$ and $|\boldsymbol{B}| > B_c$.

IV. SUMMARY AND DISCUSSION

In this paper, we have worked out solutions for two vortex molecules consisting of four half-quantized non-Abelian vortices in the neutron $^3P_2$ superfluids in the presence of the external magnetic field parallel to the angular momentum of the vortices. We have found two characteristic transitions at $|\boldsymbol{B}| < B_c$ and $|\boldsymbol{B}| \geqslant B_c$ as a result of the proximity effect between the two vortex molecules. At $0 < |\boldsymbol{B}| < B_c$, where the C-core vortex molecule with three D_4BN solitons is stabilized in the D_2BN ground state, two isolated vortex molecules dimerize through covalent bonds of D_4BN solitons namely the solitons shared by the two molecules. At $\boldsymbol{B} = 0$ where the F-core vortex molecule with a D_4BN soliton is the most stable state in the UN ground state, not only dimerization but also the transition of the vortex core state from the F state to the C state simultaneously occurs. There are also

metastable isolated C-core vortex molecules and the dimerized vortex molecule which are continuously changed from states at $0 < |\boldsymbol{B}| < B_{\rm c}$. Our results suggest that a dimerized F-core vortex molecule never exist. This situation is similar to the chemical dimerization in which two molecules having only a σ bond cannot dimerize and those having more than two bonds consisting of a σ bond and one or two π bonds can dimerize. Because the F-core vortex molecule has only one D_4BN soliton, the vortex core needs to change from F state to C state with three D_4BN solitons for isolated F-core vortex molecules to dimerize. At $|\boldsymbol{B}| \geqslant B_{\rm c}$ where the C-core vortex molecule with three D_2BN soliton is stabilized in the D_4BN ground state, no dimerization occurs. Instead, a transition of the molecule angle from $\theta_{\rm molecule} = 0$ to $\theta_{\rm molecule} = \pi/2$ occurs. The main results are summarized as the $|\boldsymbol{B}|-\Omega$ phase diagram shown in Fig. 10. We have also obtained some trimerized and tetramerized vortex molecule states as three and four vortex molecule solutions, respectively. As candidates for what happens at neutron star interiors, solutions with many vortices have also been calculated. Being different from regular triangular structure expected for singlet-pairing superfluids, the vortex configuration becomes irregular due to polymerizations of vortex molecules for $|\boldsymbol{B}| < B_{\rm c}$ and a frustration between the spatial arrangement and the internal alignments of vortex molecules for $|\boldsymbol{B}| > B_{\rm c}$.

Here, let us give discussions for future studies. We have exhausted possible two-vortex molecule states, and have briefly given some examples of three, four, and many vortex molecule states since these states are quite nontrivial. Further detailed and systematic studies should be done for a vortex-molecule lattice under a rapid rotation relevant for neutron star interiors. Athough we show the nonsymmetric configurations of vortex molecules in this work, detailed analyses are needed including comparisons with a symmetric vortex-molecule lattice as found in two-component BECs [85–87]. We here have studied only the case for the magnetic field parallel to the direction of vortices. It will be one of important directions for neutron star interiors to investigate the case of an arbitrary angle between them.

Apart from steady states under rotation studied thus far, a dynamics of vortices in three spatial dimensions is also crucial for neutron star dynamics such as pulsar glitch phenomena. The most important feature of vortex dynamics in $^3P_2$ superfluids would be the non-Abelian property of half-quantized vortices implying that they are noncommutative under exchange. It is important whether two vortices reconnect in collision or a formation of a rung between them occurs as the cases of non-Abelian vortices in the cyclic phase of a spin-2 BEC [88] and the nematic phase of a spin-2 BEC [89,90]. For instance, a vortex reconnection is crucial for states of quantum turbulences [91]. Collision of two vortex molecules may be accompanied by swapping partners as in vortex molecules in two-component BECs [92]. In addition, the dimerization of vortex molecules found in this paper may occur in a certain part of two vortex lines, thus forming for instance an X junction. Thus, multiple vortex molecules are expected to be entangled in general, which should be also crucial for pulsar glitches.

Let us mention the case of two spatial dimensions. A phase transition due to unbinding of a vortex and an antivortex is known as the Berezinskii-Kosterlitz-Thouless (BKT) transition in two spatial dimension. Recently, a novel type of BKT transition due to vortex molecules was found in two-component systems [93]. Therefore, the BKT transition of neutron $^3P_2$ superfluids confined in a quasi-two-dimensional plane should be an interesting subject.

Here, let us discuss other phases of $^3P_2$ superfluids. In this paper, we have not considered a $^1S_0$ paring, but the phase diagram under the coexistence of $^1S_0$ and $^3P_2$ superfluids is quite different from the one of solely $^3P_2$ superfluids and the most region is occupied by the D_4BN phase [94]. Vortex states in this case will be also one direction to be explored. In addition, vortex states in the ferromagnetic phase, that was found in the region close to the critical temperature without quasiclassical approximation [57], are also worth to be studied.

Quark matter consisting of diquark condensations exhibiting color superconductivity may exist in the region deeper than nuclear matter in neutron star cores. A quark-hadron continuity for two-flavor quarks was suggested to continuously connect the $^3P_2$ superfluid (nuclear matter) to a two-flavor quark matter called the 2SC + dd phase through crossover (rather than a phase transition) [95], and vortex structures in the 2SC + dd phase were studied in Refs. [96–98]. It will be interesting to study whether vortex molecule structures found in this paper is preserved or deformed through the quark-hadron continuity.

Finally, apart from $^3P_2$ superfluids, spin-2 spinor ultracold atomic BECs are also $J = 2$ condensates whose ground states are possibly nematic phase [56,90,99–102] although the current experiments of ^{87}Rb atoms imply their ground state to be in the cyclic or nematic phase [103–108]. Nematic spin-2 BECs share almost the same bosonic properties with $^3P_2$ superfluids, and thus admit the same order parameter manifold and non-Abelian half-quantized vortices [90,102]. Therefore, our present results for the dimerization of vortex molecules are also applicable to spin-2 nematic BECs which can be experimentally testable in principle.

ACKNOWLEDGMENTS

We would like to thank Yusuke Masaki for helpful discussions and comments. This work is supported in part by JSPS KAKENHI [Grants No. JP22H01221 (M.K. and M.N.), No. 20K03765 (M.K.), and No. 19KK0066 (M.K.)], the WPI program "Sustainability with Knotted Chiral Meta Matter (SKCM^2)" at Hiroshima University, and by Osaka Metropolitan University Advanced Mathematical Institute (MEXT Joint Usage/Research Center on Mathematics and Theoretical Physics JPMXP0619217849).

[1] P. Demorest, T. Pennucci, S. Ransom, M. Roberts, and J. Hessels, Nature (London) **467**, 1081 (2010).

[2] J. Antoniadis, P. C. C. Freire, N. Wex, T. M. Tauris, R. S. Lynch, M. H. van Kerkwijk, M. Kramer, C. Bassa, V. S.

Dhillon, T. Driebe, J. W. T. Hessels, V. M. Kaspi, V. I. Kondratiev, N. Langer, T. R. Marsh, M. A. McLaughlin, T. T. Pennucci, S. M. Ransom, I. H. Stairs, J. van Leeuwen *et al.*, Science **340**, 1233232 (2013).
[3] B. Abbott *et al.* (Virgo, LIGO Scientific Collaboration), Phys. Rev. Lett. **119**, 161101 (2017).
[4] B. P. Abbott *et al.* (LIGO Scientific, Virgo Collaboration), Astrophys. J. Lett. **892**, L3 (2020).
[5] T. E. Riley *et al.*, Astrophys. J. Lett. **887**, L21 (2019).
[6] M. Miller *et al.*, Astrophys. J. Lett. **887**, L24 (2019).
[7] V. Graber, N. Andersson, and M. Hogg, Int. J. Mod. Phys. D **26**, 1730015 (2017).
[8] G. Baym, T. Hatsuda, T. Kojo, P. D. Powell, Y. Song, and T. Takatsuka, Rep. Prog. Phys. **81**, 056902 (2018).
[9] A. B. Migdal, Zh. Eksp. Teor. Fiz. **37**, 249 (1960) [Sov. Phys. JETP **10**, 176 (1960)].
[10] N. Chamel and P. Haensel, Living Rev. Relativity **11**, 10 (2008).
[11] N. Chamel, J. Astrophys. Astron. **38**, 43 (2017).
[12] B. Haskell and A. Sedrakian, in *The Physics and Astrophysics of Neutron Stars*, Astrophysics and Space Science Library, Vol. 457, edited by L. Rezzolla, P. Pizzochero, D. Jones, N. Rea, and I. Vidaña (Springer, Cham, 2018), pp. 401–454.
[13] A. Sedrakian and J. W. Clark, Eur. Phys. J. A **55**, 167 (2019).
[14] N. Andersson, Universe **7**, 17 (2021).
[15] G. Baym, C. Pethick, D. Pines, and M. Ruderman, Nature (London) **224**, 872 (1969).
[16] D. Pines, J. Shaham, and M. Ruderman, Nat. Phys. Sci. **237**, 83 (1972).
[17] T. Takatsuka and R. Tamagaki, Prog. Theor. Phys. **79**, 274 (1988).
[18] D. G. Yakovlev, A. D. Kaminker, O. Y. Gnedin, and P. Haensel, Phys. Rep. **354**, 1 (2001).
[19] A. Y. Potekhin, J. A. Pons, and D. Page, Space Sci. Rev. **191**, 239 (2015).
[20] D. G. Yakovlev, K. P. Levenfish, and Yu. A. Shibanov, Phys. Usp. **42**, 737 (1999).
[21] C. O. Heinke and W. C. G. Ho, Astrophys. J. Lett. **719**, L167 (2010).
[22] P. S. Shternin, D. G. Yakovlev, C. O. Heinke, W. C. G. Ho, and D. J. Patnaude, Mon. Not. R. Astron. Soc.: Lett. **412**, L108 (2011).
[23] D. Page, M. Prakash, J. M. Lattimer, and A. W. Steiner, Phys. Rev. Lett. **106**, 081101 (2011).
[24] P. E. Reichley and G. S. Downs, Nat. Phys. Sci. **234**, 48 (1971).
[25] P. W. Anderson and N. Itoh, Nature (London) **256**, 25 (1975).
[26] R. A. Wolf, Astrophys. J. **145**, 834 (1966).
[27] F. Tabakin, Phys. Rev. **174**, 1208 (1968).
[28] M. Hoffberg, A. E. Glassgold, R. W. Richardson, and M. Ruderman, Phys. Rev. Lett. **24**, 775 (1970).
[29] R. Tamagaki, Prog. Theor. Phys. **44**, 905 (1970).
[30] T. Takatsuka and R. Tamagaki, Prog. Theor. Phys. **46**, 114 (1971).
[31] T. Takatsuka, Prog. Theor. Phys. **47**, 1062 (1972).
[32] T. Fujita and T. Tsuneto, Prog. Theor. Phys. **48**, 766 (1972).
[33] R. W. Richardson, Phys. Rev. D **5**, 1883 (1972).
[34] L. Amundsen and E. Østgaard, Nucl. Phys. A **442**, 163 (1985).
[35] T. Takatsuka and R. Tamagaki, Prog. Theor. Phys. Suppl. **112**, 27 (1993).
[36] M. Baldo, J. Cugnon, A. Lejeune, and U. Lombardo, Nucl. Phys. A **536**, 349 (1992).
[37] Ø. Elgarøy, L. Engvik, M. Hjorth-Jensen, and E. Osnes, Nucl. Phys. A **607**, 425 (1996).
[38] V. A. Khodel, V. V. Khodel, and J. W. Clark, Phys. Rev. Lett. **81**, 3828 (1998).
[39] M. Baldo, O. Elgaroy, L. Engvik, M. Hjorth-Jensen, and H. J. Schulze, Phys. Rev. C **58**, 1921 (1998).
[40] V. V. Khodel, V. A. Khodel, and J. W. Clark, Nucl. Phys. A **679**, 827 (2001).
[41] M. V. Zverev, J. W. Clark, and V. A. Khodel, Nucl. Phys. A **720**, 20 (2003).
[42] S. Maurizio, J. W. Holt, and P. Finelli, Phys. Rev. C **90**, 044003 (2014).
[43] S. K. Bogner, R. J. Furnstahl, and A. Schwenk, Prog. Part. Nucl. Phys. **65**, 94 (2010).
[44] S. Srinivas and S. Ramanan, Phys. Rev. C **94**, 064303 (2016).
[45] M. Stein, A. Sedrakian, X.-G. Huang, and J. W. Clark, Phys. Rev. C **93**, 015802 (2016).
[46] N. D. Mermin, Phys. Rev. A **9**, 868 (1974).
[47] J. A. Sauls and J. W. Serene, Phys. Rev. D **17**, 1524 (1978).
[48] P. Muzikar, J. A. Sauls, and J. W. Serene, Phys. Rev. D **21**, 1494 (1980).
[49] J. A. Sauls, D. L. Stein, and J. W. Serene, Phys. Rev. D **25**, 967 (1982).
[50] V. Z. Vulovic and J. A. Sauls, Phys. Rev. D **29**, 2705 (1984).
[51] K. Masuda and M. Nitta, Phys. Rev. C **93**, 035804 (2016).
[52] K. Masuda and M. Nitta, Prog. Theor. Exp. Phys. **2020**, 013D01 (2020).
[53] S. Yasui, C. Chatterjee, and M. Nitta, Phys. Rev. C **99**, 035213 (2019).
[54] S. Yasui, C. Chatterjee, and M. Nitta, *Proceedings of the 8th International Conference on Quarks and Nuclear Physics (QNP2018): Tsukuba, Japan, November 13–17, 2018*, JPS Conf. Proc. **26**, 024022 (2019).
[55] S. Yasui, C. Chatterjee, M. Kobayashi, and M. Nitta, Phys. Rev. C **100**, 025204 (2019).
[56] M. Kobayashi and M. Nitta, Phys. Rev. A **104**, 053302 (2021).
[57] T. Mizushima, S. Yasui, D. Inotani, and M. Nitta, Phys. Rev. C **104**, 045803 (2021).
[58] P. F. Bedaque, G. Rupak, and M. J. Savage, Phys. Rev. C **68**, 065802 (2003).
[59] L. B. Leinson, Phys. Lett. B **702**, 422 (2011).
[60] L. B. Leinson, Phys. Rev. C **85**, 065502 (2012).
[61] L. B. Leinson, Phys. Rev. C **87**, 025501 (2013).
[62] P. F. Bedaque and A. N. Nicholson, Phys. Rev. C **87**, 055807 (2013); **89**, 029902(E) (2014).
[63] P. Bedaque and S. Sen, Phys. Rev. C **89**, 035808 (2014).
[64] P. F. Bedaque and S. Reddy, Phys. Lett. B **735**, 340 (2014).
[65] P. F. Bedaque, A. N. Nicholson, and S. Sen, Phys. Rev. C **92**, 035809 (2015).
[66] L. B. Leinson, Phys. Rev. C **81**, 025501 (2010).
[67] L. B. Leinson, Phys. Lett. B **689**, 60 (2010).
[68] L. B. Leinson, Phys. Rev. C **82**, 065503 (2010); **84**, 049901(E) (2011).
[69] L. B. Leinson, Phys. Rev. C **83**, 055803 (2011).
[70] L. B. Leinson, Phys. Rev. C **84**, 045501 (2011).
[71] S. Yasui and M. Nitta, Phys. Rev. C **101**, 015207 (2020).
[72] S. Yasui, C. Chatterjee, and M. Nitta, Phys. Rev. C **101**, 025204 (2020).
[73] T. Mizushima, K. Masuda, and M. Nitta, Phys. Rev. B **95**, 140503(R) (2017).

[74] T. Mizushima, S. Yasui, and M. Nitta, Phys. Rev. Res. **2**, 013194 (2020).
[75] Y. Masaki, T. Mizushima, and M. Nitta, Phys. Rev. Res. **2**, 013193 (2020).
[76] Y. Masaki, T. Mizushima, and M. Nitta, Phys. Rev. B **105**, L220503 (2022).
[77] A. P. Schnyder, S. Ryu, A. Furusaki, and A. W. W. Ludwig, Phys. Rev. B **78**, 195125 (2008).
[78] S. Ryu, A. P. Schnyder, A. Furusaki, and A. W. W. Ludwig, New J. Phys. **12**, 065010 (2010).
[79] C. Chatterjee, M. Haberichter, and M. Nitta, Phys. Rev. C **96**, 055807 (2017).
[80] M. Kobayashi and M. Nitta, Phys. Rev. C **105**, 035807 (2022).
[81] L. B. Leinson, Mon. Not. R. Astron. Soc. **498**, 304 (2020).
[82] G. Marmorini, S. Yasui, and M. Nitta, arXiv:2010.09032.
[83] S. Kobayashi, M. Kobayashi, Y. Kawaguchi, M. Nitta, and M. Ueda, Nucl. Phys. B **856**, 577 (2012).
[84] M. M. Salomaa and G. E. Volovik, Phys. Rev. B **31**, 203 (1985).
[85] E. J. Mueller and T.-L. Ho, Phys. Rev. Lett. **88**, 180403 (2002).
[86] K. Kasamatsu, M. Tsubota, and M. Ueda, Phys. Rev. Lett. **91**, 150406 (2003).
[87] M. Cipriani and M. Nitta, Phys. Rev. Lett. **111**, 170401 (2013).
[88] M. Kobayashi, Y. Kawaguchi, M. Nitta, and M. Ueda, Phys. Rev. Lett. **103**, 115301 (2009).
[89] M. Kobayashi, Y. Kawaguchi, and M. Ueda, arXiv:0907.3716.
[90] M. O. Borgh and J. Ruostekoski, Phys. Rev. Lett. **117**, 275302 (2016); **118**, 129901(E) (2017).
[91] M. Kobayashi and M. Ueda, arXiv:1606.07190.
[92] M. Eto, K. Ikeno, and M. Nitta, Phys. Rev. Res. **2**, 033373 (2020).
[93] M. Kobayashi, M. Eto, and M. Nitta, Phys. Rev. Lett. **123**, 075303 (2019).
[94] S. Yasui, D. Inotani, and M. Nitta, Phys. Rev. C **101**, 055806 (2020).
[95] Y. Fujimoto, K. Fukushima, and W. Weise, Phys. Rev. D **101**, 094009 (2020).
[96] Y. Fujimoto and M. Nitta, Phys. Rev. D **103**, 054002 (2021).
[97] Y. Fujimoto and M. Nitta, Phys. Rev. D **103**, 114003 (2021).
[98] Y. Fujimoto and M. Nitta, J. High Energy Phys. 09 (2021) 192.
[99] F. Zhou and G. W. Semenoff, Phys. Rev. Lett. **97**, 180411 (2006).
[100] G. W. Semenoff and F. Zhou, Phys. Rev. Lett. **98**, 100401 (2007).
[101] S. Uchino, M. Kobayashi, and M. Ueda, Phys. Rev. A **81**, 063632 (2010).
[102] S. Uchino, M. Kobayashi, M. Nitta, and M. Ueda, Phys. Rev. Lett. **105**, 230406 (2010).
[103] H. Schmaljohann, M. Erhard, J. Kronjäger, M. Kottke, S. van Staa, L. Cacciapuoti, J. J. Arlt, K. Bongs, and K. Sengstock, Phys. Rev. Lett. **92**, 040402 (2004).
[104] M.-S. Chang, C. D. Hamley, M. D. Barrett, J. A. Sauer, K. M. Fortier, W. Zhang, L. You, and M. S. Chapman, Phys. Rev. Lett. **92**, 140403 (2004).
[105] T. Kuwamoto, K. Araki, T. Eno, and T. Hirano, Phys. Rev. A **69**, 063604 (2004).
[106] A. Widera, F. Gerbier, S. Fölling, T. Gericke, O. Mandel, and I. Bloch, New J. Phys. **8**, 152 (2006).
[107] S. Tojo, A. Tomiyama, M. Iwata, T. Kuwamoto, and T. Hirano, Appl. Phys. B **93**, 403 (2008).
[108] S. Tojo, T. Hayashi, T. Tanabe, T. Hirano, Y. Kawaguchi, H. Saito, and M. Ueda, Phys. Rev. A **80**, 042704 (2009).
[109] E. Babaev, Phys. Rev. Lett. **89**, 067001 (2002).
[110] E. Babaev, A. Sudbo, and N. W. Ashcroft, Nature (London) **431**, 666 (2004).
[111] J. Goryo, S. Soma, and H. Matsukawa, Europhys. Lett. **80**, 17002 (2007).
[112] Y. Tanaka, A. Crisan, D. D. Shivagan, A. Iyo, K. Tokiwa, and T. Watanabe, Jpn. J. Appl. Phys. **46**, 134 (2007).
[113] A. Crisan, Y. Tanaka, D. D. Shivagan, A. Iyo, L. Cosereanu, K. Tokiwa, and T. Watanabe, Jpn. J. Appl. Phys. **46**, L451 (2007).
[114] J. W. Guikema, H. Bluhm, D. A. Bonn, R. Liang, W. N. Hardy, and K. A. Moler, Phys. Rev. B **77**, 104515 (2008).
[115] M. Nitta, M. Eto, T. Fujimori, and K. Ohashi, J. Phys. Soc. Jpn. **81**, 084711 (2012).
[116] J. Garaud, J. Carlstrom, and E. Babaev, Phys. Rev. Lett. **107**, 197001 (2011).
[117] J. Garaud, J. Carlström, E. Babaev, and M. Speight, Phys. Rev. B **87**, 014507 (2013).
[118] J. Garaud and E. Babaev, Phys. Rev. B **86**, 060514(R) (2012).
[119] Y. Tanaka, H. Yamamori, T. Yanagisawa, T. Nishio, and S. Arisawa, Physica C **538**, 12 (2017).
[120] Y. Tanaka, H. Yamamori, T. Yanagisawa, T. Nishio, and S. Arisawa, Physica C **548**, 44 (2018).
[121] C. Chatterjee, S. B. Gudnason, and M. Nitta, J. High Energy Phys. 04 (2020) 109.
[122] J. Garaud, arXiv:2203.12194.
[123] D. T. Son and M. A. Stephanov, Phys. Rev. A **65**, 063621 (2002).
[124] K. Kasamatsu, M. Tsubota, and M. Ueda, Phys. Rev. Lett. **93**, 250406 (2004).
[125] P. Kuopanportti, J. A. M. Huhtamäki, and M. Möttönen, Phys. Rev. A **85**, 043613 (2012).
[126] A. Aftalion, P. Mason, and J. Wei, Phys. Rev. A **85**, 033614 (2012).
[127] M. Eto and M. Nitta, Phys. Rev. A **85**, 053645 (2012).
[128] M. Eto and M. Nitta, Europhys. Lett. **103**, 60006 (2013).
[129] M. Nitta, M. Eto, and M. Cipriani, J. Low Temp. Phys. **175**, 177 (2014).
[130] D. S. Dantas, A. R. P. Lima, A. Chaves, C. A. S. Almeida, G. A. Farias, and M. V. Milošević, Phys. Rev. A **91**, 023630 (2015).
[131] M. Tylutki, L. P. Pitaevskii, A. Recati, and S. Stringari, Phys. Rev. A **93**, 043623 (2016).
[132] M. Eto and M. Nitta, Phys. Rev. A **97**, 023613 (2018).
[133] B. Mencia Uranga and A. Lamacraft, Phys. Rev. A **97**, 043609 (2018).
[134] M. Eto and M. Nitta, Phys. Rev. D **104**, 094052 (2021).
[135] M. Eto, Y. Hamada, and M. Nitta, J. High Energy Phys. 02 (2022) 99.